

# Symmetric Sliding-Mode Control of Grid-Forming Inverters With Controllable Region Under AC and DC Sides Varying

Qianxi Tang, *Graduate Student Member, IEEE*, Li Peng, *Senior Member, IEEE*

Post Conference Paper [DELETE THIS LINE FROM YOUR ACCEPTED FINAL SUBMISSION]

**Abstract**—Conventional grid-forming (GFM) controls often entangle voltage formation with power flow and dc-source dynamics, which can degrade voltage tracking performance and stability under grid disturbances, load transients, and dc-side perturbations. To address this issue, a symmetric sliding-mode control (SSMC) method is developed and its explicit voltage controllable region is derived. It illustrates how much ac-side power dynamics and dc-link voltage varying can be decoupled from the voltage regulation task, which helps predict when the entangling appears. While conventional sliding-mode controls address voltage-tracking error through complex sliding surface designs, repetitive correction techniques or special reaching laws, this work identifies that the error at power-line frequency primarily stem from the asymmetry property of inverters with the delay effect and the computational inaccuracy. Guided by this insight, a symmetric compensation structure is proposed, which avoids added design complexity and directly mitigates low-frequency voltage tracking errors. Furthermore, the control design is supported by a physical and quantitative explanation, aiding in parameter tuning. Simulation and experimental results demonstrate that the proposed method achieves faster tracking responses on the order of hundreds of microseconds while maintaining robust and more accurate tracking under both dc-link voltage and ac-side current variations. Conventional grid-forming and classical sliding-mode controllers, which handle these disturbances separately, cannot match this combined speed and robustness. Furthermore, the voltage controllability analysis is explicitly verified.

**Index Terms**—AC-current changing, dc-link voltage, grid-forming inverters (GFMI), sliding-mode control, voltage regulation

## I. INTRODUCTION

GRID-forming inverters are interfaces between the modern grid and renewable or power storage devices to regulate the ac-side voltage. Because of the modern grid which is composed of more distributed power sources, fewer large-inertia synchronous generators and intermittent nature of wind and solar resources etc., dc-link voltage and ac-side power dynamics become more sophisticated. Therefore, how this grid-forming interface technology stably provides voltage regulation service, regardless of the significantly fluctuating

from dc-link voltage and ac-side current, becomes a serious challenge. Therefore, some new voltage controllers are proposed to achieve good voltage tracking, significantly varying operating-point condition, wide stability-range robustness [1]–[3]. Nevertheless, voltage tracking is slow and exists error in low-frequency and voltage-forming accuracy is coupled with power injection to grid, which might damage the performance of synchronous loop. Furthermore, these methods haven't provided the voltage controllable region related to its dc-voltage level and ac-current changing rate explicitly. This omission makes it difficult to assess under what conditions a voltage regulation strategy will fail and what the voltage trajectory could be when the inverter is outside the voltage controllable region. As a result, the stability of a GFMI becomes an issue that the voltage loop and the synchronization loop are intricately interacted [4], which is hard to be analyzed. It remains unclear whether failure arises primarily from poor voltage tracking or loss of synchronization, and in many cases, failures are attributed to both simultaneously without identifying the dominant cause [5]. The confusion is further compounded in studies that assume ideal voltage control, i.e., perfect voltage tracking [6].

While some recent methods attempt to regulate the dc-link voltage to support ac-side voltage stability under large states' varying [7], this often comes at the cost of reduced voltage regulation capability at the point of common coupling (PCC). For instance, strict dc-voltage level regulation can limit the controllability of either the voltage magnitude or the frequency [8], [9]. This trade-off raises a critical question: rather than enforcing tight dc-voltage regulation, why not consider how much dc-voltage variation the voltage controller can tolerate while still maintaining robust and accurate ac-voltage regulation?

To achieve accurate and robust voltage tracking, and to analyze the voltage controllable boundary condition, a sliding-mode control (SMC) strategy rooted in nonlinear system analysis is employed. Because the scheme derives the voltage-controllable region in closed form, the tracking accuracy and convergence speed can be rigorously quantified. Furthermore, the analysis shows that the voltage controllable region is a time function of dc-voltage level and ac-current changing rate, which means the answer of how much dc-voltage variation the

voltage controller can tolerate while still maintaining robust and accurate ac-voltage regulation is given in this condition. However, conventional sliding-mode voltage control for grid-forming inverters rarely connect the discrete switching action of the power stage with the reaching law. To address it, designers introduce higher-order or adaptive sliding surfaces and bespoke reaching laws, but the resulting schemes still fall short of microsecond-level settling and leave a discernible 50/60 Hz residual [10], [11]. The proliferation of auxiliary gains also obscures the physical link between each parameter and the inverter's energy-conversion process, forcing practitioners to rely on empirical tuning rather than first principles.

This paper proposes a symmetric sliding-mode voltage control combined a physical and quantitative explanation of control design. The main contributions are as follows:

- 1) A symmetric sliding-mode control is proposed and can achieve microsecond-scale response and suppressed voltage error which appears in many traditional sliding-mode controls. Unlike conventional grid-forming and sliding-mode controllers, which address dc-bus or ac-current disturbances in isolation, the proposed SSMC maintains tighter and more robust voltage tracking under simultaneous dc-link-voltage and ac-side-current variations. The controller's physically grounded parameter choosing guarantees accurate voltage formation even under large ac and dc variations.
- 2) The explicit voltage controllable region is introduced, showing the inverter's dynamic tracking speed and accuracy is determined by both ac-current changing rate and dc-voltage level. It helps predict when the entangling severely appears and how much ac-side power dynamics and dc-link voltage varying can be decoupled from the voltage regulation task.
- 3) The experimental data confirms that, when operating within the voltage-controllable region, the system achieves fast and accurate voltage tracking with a well-defined convergence rate and steady-state error. This behavior lays a practical foundation for modeling the voltage control loop as a reliable subsystem for higher-level control analysis, such as synchronization loop design.

## II. SYMMETRIC SLIDING-MODE CONTROL WITH VOLTAGE CONTROLLABLE REGION

The diagram and control architecture of the GFMI system is shown in Fig. 1. The topology of the three-phase voltage source inverter is chosen to be the prototype. With three-phase balanced condition, the equivalent single-phase model in Fig. 2 is adopted for the analysis [12]. Then, the other two can use the same analysis following below [13]. Background on sliding-mode control can be found in [14]–[16].

$$\begin{aligned} L_f \frac{di_f}{dt} &= T v_{dc} - u_o \\ C_f \frac{du_o}{dt} &= i_f - i_o \end{aligned} \quad (1)$$

Fig. 2 illustrates an inverter system with a dc-link, an LC filter and a transmission line. In its dynamic equation (1), the

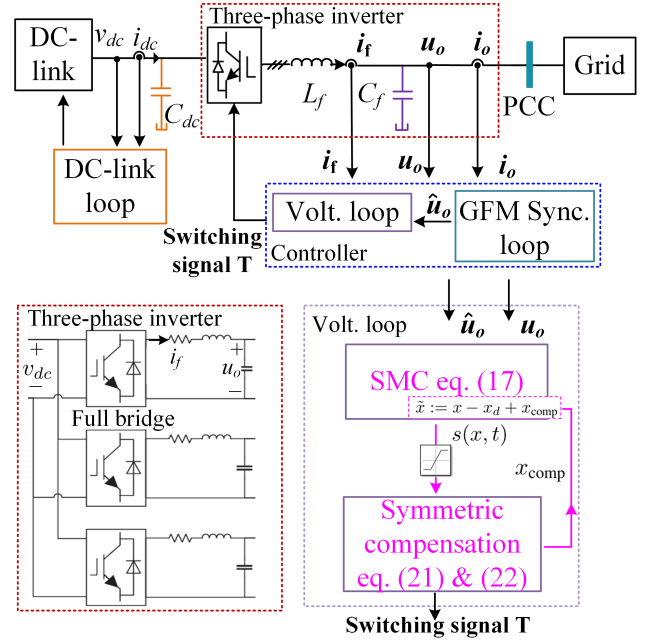


Fig. 1. The diagram and control architecture of the GFMI system.

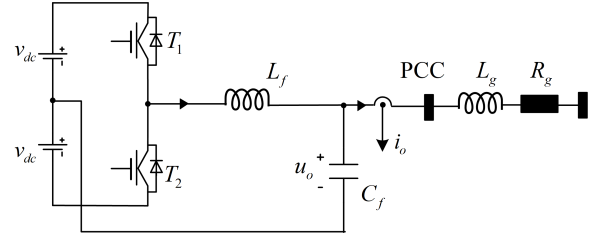


Fig. 2. The equivalent one phase inverter.

variables are capacitor voltage  $u_o$ , output current  $i_o$ , switching variable  $T$ , dc-link  $v_{dc}$ . When  $T_1$  is on,  $T = 1$ . When  $T_2$  is on,  $T = -1$ . The variable  $i_f$  is now eliminated, the term  $T v_{dc}$  is replaced with control input  $u$ , and the terms  $u_o$  and  $i_o$  are combined into one system function  $f(u_o, i_o)$  in (2).

$$\begin{aligned} \frac{d^2 u_o}{dt^2} &= -\frac{u_o}{L_f C_f} - \frac{1}{C_f} \frac{di_o}{dt} + \frac{T v_{dc}}{L_f C_f} \\ \frac{d^2 u_o}{dt^2} &= -\frac{u_o}{L_f C_f} - \frac{1}{C_f} \frac{di_o}{dt} + u = f(u_o, i_o) + u \end{aligned} \quad (2)$$

Note that it's a second order system. The  $f$  and  $u$  are like forces changing the displacement vector,  $u_o$ . The  $i_o$  here is the current injected into grid side and is known and measured by sensor.

Now, the sliding-mode control can be derived. First, define the tracking error in (3), where  $x = u_o$  and  $x_d, u_d$  are the desired output-voltage trajectory. Furthermore, define  $s$  in (3).

$$\begin{aligned} \tilde{x} &:= x - x_d = u_o - u_d \\ s(x, t) &:= \left( \frac{d}{dt} + \lambda \right) \tilde{x} \end{aligned} \quad (3)$$

A conclusion [14] is that bounds on  $s$  can directly translated into bounds on the tracking error vector  $\tilde{x}$ , when the initial

tracking error is 0, given as

$$\forall t \geq 0, |s(t)| \leq \Phi \Rightarrow \forall t \geq 0, |\tilde{x}| \leq \frac{\Phi}{\lambda} \quad (4)$$

where  $\lambda$  is a strictly positive constant parameter. The physical meaning is that filtering the  $s$  chattering using  $\lambda$  makes the  $\tilde{x}$  zero. So, the  $\lambda$  should be high enough to filter the direct component of  $s$  and low enough to filter out the switching ripple of  $s$ , typically  $\lambda = \frac{\text{Switching frequency}}{5}$  [14]. And the initial zero tracking condition [14] is guaranteed by

$$\frac{1}{2} \frac{d}{dt} s^2 \leq -\eta |s| \quad (5)$$

where the  $\eta$  is a strictly positive constant representing the desired lowest converging speed, which guarantees the finite-time convergence. The derivative of  $s$  is

$$\dot{s} = f - \ddot{x}_d + \lambda \dot{\tilde{x}} + u. \quad (6)$$

Using the average model [17], the modulation waveform could be chosen as ideal control input  $u_{ideal}$  in (7).

$$u_{ideal} = -\hat{f} + \ddot{x}_d - \lambda \dot{\tilde{x}} - (F + \eta) \text{sgn}(s) \quad (7)$$

where  $|\hat{f} - f| \leq F$ .  $\hat{f}$  is the estimated model, whereas  $f$  is the true, perfectly accurate model.  $F$  represents modeling uncertainty [14]. The reason of (7) as control law works, is that the control input is an averaged discontinuous value, which is a function of  $v_{dc}$ , so the nature of this inverter system is a variable structure system corresponding to the discontinuous switching behaviors of the bridge arms. When  $x$  is around a desired trajectory, the forces to change inverter states are discontinuously up and down crossing the desired trajectory to make the system have the freedom to move along the desired trajectory. With this understanding, the voltage controllable region is naturally obtained in (8), where  $g(x) = \frac{x}{L_f C_f}$ , to satisfy contraction to  $s$  surface condition [18].

$$\begin{aligned} u = g(-v_{dc}) &\leq -\hat{f} + \ddot{x}_d - \lambda \dot{\tilde{x}} - (F + \eta), s > 0 \\ u = g(+v_{dc}) &\geq -\hat{f} + \ddot{x}_d - \lambda \dot{\tilde{x}} + (F + \eta), s < 0 \end{aligned} \quad (8)$$

*Proof.* Case  $s > 0$ . Apply the first line of (8):

$$u \leq -\hat{f} + \ddot{x}_d - \lambda \dot{\tilde{x}} - (F + \eta).$$

Substituting into (6), gives

$$\dot{s} \leq (f - \hat{f}) - (F + \eta) \leq -\eta,$$

because  $|\hat{f} - f| \leq F$ .

Case  $s < 0$ . Use the second line of (8):

$$u \geq -\hat{f} + \ddot{x}_d - \lambda \dot{\tilde{x}} + (F + \eta),$$

which yields

$$\dot{s} \geq (f - \hat{f}) + (F + \eta) \geq +\eta,$$

since  $|\hat{f} - f| \leq F$ .

Define the Lyapunov candidate  $V = \frac{1}{2} s^2$ . Then  $\dot{V} = s \dot{s}$ , and the two cases above imply

$$\dot{V} = \frac{1}{2} \frac{d}{dt} s^2 \leq -\eta |s|,$$

which is exactly (5).

In both cases we have  $\dot{V} = s \dot{s} \leq -\eta |s|$ . Because  $\dot{V}$  is negative definite outside  $s = 0$ , standard finite-time convergence results for first-order sliding surfaces imply reachability in time less than  $|s(0)|/\eta$ .  $\square$

Therefore, only when the (8) is satisfied, both the desired converging speed  $\eta$  and voltage controllability is guaranteed. This boundary condition tells when the voltage regulation control would lose controllability. It shows that the voltage controllability is related to the desired trajectory, the output current changing rate, the inductor, modeling uncertainty, required convergence speed and the dc-link voltage level. It also illustrates that the voltage controllability depends on the inverter's hardware and the desired performance requirements, rather than on the specified controller type. It is proved that (3) is a bijection [19]. So, the controllability of  $s$  is the controllability of  $\tilde{x}$ .

### A. Voltage-Controllability Region

The inverter's ability to follow a voltage reference is restricted by the controllability window (8), which can be written as (9).

$$\left| \ddot{u}_d + \frac{u_o}{L_f C_f} + \frac{1}{C_f} \frac{di_o}{dt} + \lambda \dot{\tilde{x}} \right| \leq \frac{v_{dc}}{L_f C_f} - (F + \eta) \quad (9)$$

However, this controllability region is not directly related to inverter states, which is not convenient to determine whether the voltage is controllable or not under different application scenarios. If the  $\dot{\tilde{x}}$  term is replaced by the inverter states, that goal can be realized.

a) *Step 1: express  $\dot{\tilde{x}}$  through  $s$  and  $\tilde{x}$ :* By definition of the sliding surface,

$$s = \dot{\tilde{x}} + \lambda \tilde{x} \implies \dot{\tilde{x}} = s - \lambda \tilde{x}. \quad (10)$$

b) *Step 2: apply the triangle inequality:*

$$|\dot{\tilde{x}}| \leq |s| + \lambda |\tilde{x}|. \quad (11)$$

c) *Step 3: insert a state bound obtained from the reaching law:* Using the reaching inequality  $\frac{1}{2} \dot{s}^2 \leq -\eta |s|$  together with (10) one show

$$|\tilde{x}| \leq \frac{|s|}{\lambda} + \frac{\eta}{\lambda^2}. \quad (12)$$

Substituting (12) into (11) yields

$$\begin{aligned} |\dot{\tilde{x}}| &\leq |s| + \lambda \left( \frac{|s|}{\lambda} + \frac{\eta}{\lambda^2} \right) \\ &= 2|s| + \frac{\eta}{\lambda}. \end{aligned} \quad (13)$$

d) *Step 4: eliminate  $|s(t)|$  with its worst-case decay:* From  $\frac{1}{2} \dot{s}^2 \leq -\eta |s|$  we have

$$|s(t)| \leq |s(t_0)| - \eta(t - t_0), \quad t_0 \leq t \leq t_0 + |s(t_0)|/\eta. \quad (14)$$

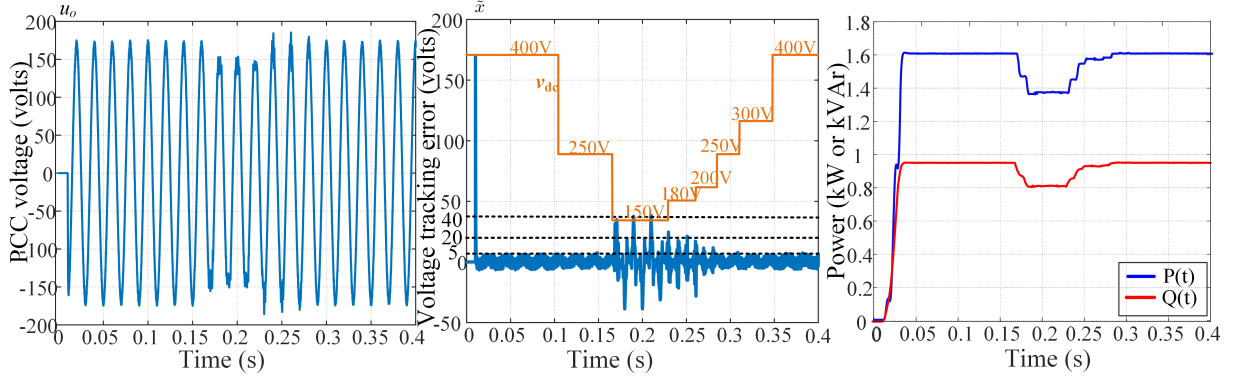


Fig. 3. Simulation to examine voltage controllability varying  $v_{dc}$  from 150V to 400V.

e) *Step 5: Final form (no  $\dot{x}$  term)*: Inserting (14) into (13) gives the explicit time-dependent bound of  $|\hat{x}(t)|$ .

$$\begin{aligned} |\dot{\hat{x}}(t)| &\leq 2(|s(t_0)| - \eta(t - t_0)) + \frac{\eta}{\lambda}, \\ t_0 \leq t \leq t_0 + \frac{|s(t_0)|}{\eta}. \end{aligned} \quad (15)$$

Inserting (15) into (9) gives the final form of voltage controllability.

$$\begin{aligned} \left| \ddot{u}_d + \frac{u_o}{L_f C_f} + \frac{1}{C_f} \frac{di_o}{dt} \right| &\leq \frac{v_{dc}}{L_f C_f} - (F + 2\eta) \\ &\quad - 2\lambda(|s(t_0)| - \eta(t - t_0)), \\ t_0 \leq t \leq t_0 + \frac{|s(t_0)|}{\eta}. \end{aligned} \quad (16)$$

The transient term  $-2\lambda(|s(t_0)| - \eta(t - t_0))$  is most negative at  $t = t_0$  and relaxes linearly to zero as  $|s(t)|$  collapses; hence a design with a modest  $\eta$  may momentarily violate the bound at start-up, yet satisfy it automatically a few switching cycles later. Conversely, selecting a larger  $\eta$  widens the static deduction  $F + 2\eta$  but shortens the reaching interval  $|s(t_0)|/\eta$ . Once the surface is around ( $s \rightarrow 0$ ) the transient offset disappears and the right hand side of the inequality (16) reduces to  $\frac{v_{dc}}{L_f C_f} - (F + 2\eta)$ . The simulation is given in this section B to check its effectiveness after the control law is provided.

### B. The Asymmetry and the Symmetric Control

Different from the traditional sliding-mode control methods which improve the tracking performance by using advanced sliding surfaces and reaching laws, this paper will find the root of the asymmetry problem causing an error when it is tracking a trajectory. The dynamic of  $s$  is in (17) and (18), when the hysteresis function is used to generate switching signals. The hysteresis function meets (8) outside its band, which guarantees the convergence to the sliding surface.

$$\dot{s} = f - \ddot{x}_d + \lambda \dot{x} + \frac{v_{dc} \text{hysteresis}(\frac{-s}{h})}{L_f C_f} \quad (17)$$

$$s_n - s_{n-1} = \dot{s}_{n-1} \times t_{di} \quad (18)$$

Equation (17) and (18) show that the dynamic of  $s$  is related to the decision interval  $t_{di}$ , namely the switching interval (combining the delay effect and computational error in Fig. 4), since the controller is a digital one. Now, let's consider the asymmetric dynamic of sliding mode control. The modeling is thought to be accurate, so  $F=0$ . Moreover, it is sufficient to require that  $\eta$  is positive. When the voltage state is close to sliding surface, the orders of  $i_o$  magnitude is several tens of amperes, and the value of  $L_f$  is several millihenries, the  $u_o$  and  $i_o$  terms are the dominant term that affects the  $s$  dynamics.

Therefore,

$$\dot{s}_{n-1} \approx -\frac{u_o}{L_f C_f} - \frac{1}{C_f} \frac{di_o}{dt} \pm v_{dc}. \quad (19)$$

When  $\frac{x}{L_f C_f} + \frac{1}{C_f} \frac{di_o}{dt}$  is at positive half cycle, the  $s$  has an average down velocity tendency during a switching cycle because of the decision time or switching interval. Whenever the  $\pm v_{dc}$  changes the sign, after a  $t_{di}$  of the digital controller, the velocity of  $s$  would change to another value. As a result, the  $s$  dynamics is asymmetric across the  $s$  surface.

The simulation verifies the claim above where a one phase inverter is controlled by a conventional sliding-mode and connected with a load. The parameter setting is on Table I. Fig. 3 shows the effectiveness of (16) to predict the voltage controllable region with  $v_{dc}$  changing. By (16), dc-link voltage level should be higher than  $(110 + 20) * 1.414 = 181\text{volts}$ , which is coherent to the simulation result in Fig. 3, otherwise there is undesired loss of injected power and distorted output-voltage waveform. It also shows when the inverter is in the voltage controllable region the accuracy, the injected power to grid don't change anymore. This gives the explicit interaction mechanism between the synchronous reference signal and voltage formation loop with this boundary condition. During  $v_{dc}$  changes from 400V to 250V at 0.2 seconds, the condition (16) is always satisfied. In Fig. 4, the  $s$  isn't contained in the hysteresis boundary. Within the condition (16), point C illustrates that it is not the system not controllable, but it is that the  $s$  plot is wrong, which is called the computational error. The delay effect arrow shows that the  $t_{di}$  is also important to the error of  $s$ .



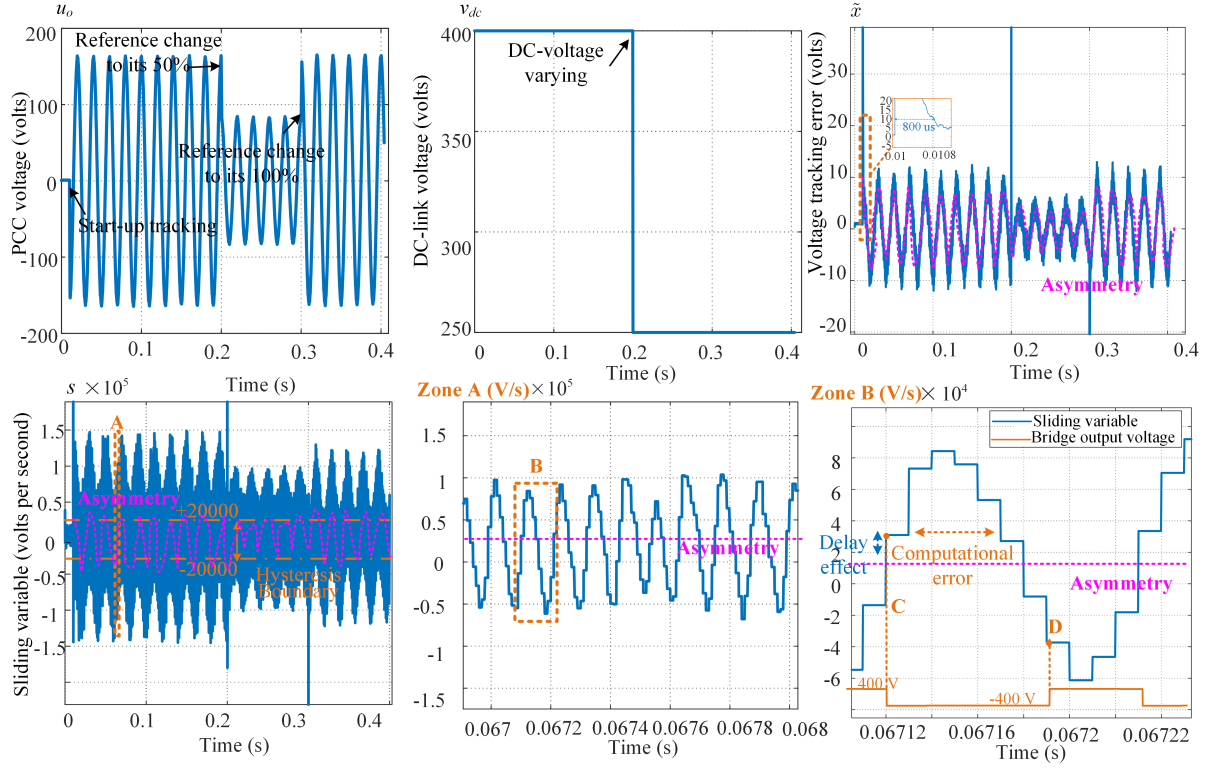


Fig. 4. The simulation result of asymmetry when  $t_{di} = 10 \mu s$ , with a reference magnitude that steps from 100% to 50% at 0.2s with dc-voltage jump from 400V to 250V for examining the  $v_{dc}$  varying resilience and then back to 100% at 0.3s.

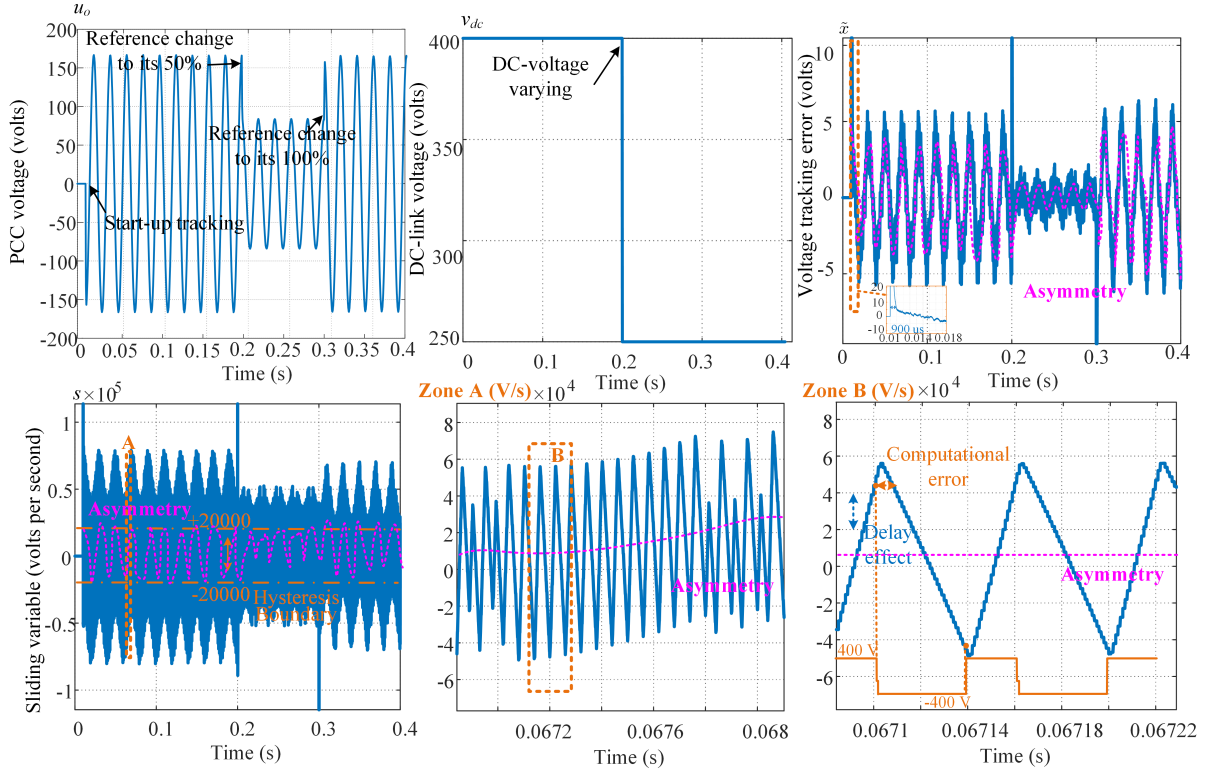


Fig. 5. The simulation result of asymmetry when  $t_{di} = 2 \mu s$ , with a reference magnitude that steps from 100% to 50% at 0.2s with dc-voltage jump from 400V to 250V for examining  $v_{dc}$  varying resilience and then back to 100% at 0.3s.

TABLE I  
PARAMETERS OF SIMULATION AND EXPERIMENTAL SETUPS

Symbol	Description	Value
$f_n$	Nominal frequency	$100\pi$ rad/s
$S_n$	Nominal power	5 kW
$V_n$	Nominal one phase RMS voltage	110 V
$C_f$	Filter capacitor	330 $\mu$ F
$L_f$	Filter inductor	0.3 mH
$v_{dc}$	Nominal dc-link voltage	400 V
$P_{load}$	Simulation active power	1600 W
$Q_{load}$	Simulation reactive power	800 VAR
$\lambda$	Sliding control parameters	4480 /s
$h$	Simulation hysteresis band	20000 V/s
$\omega_0$	Natural frequency	314.16 rad/s
$\zeta$	Simulation damping ratio	20
$P_{step}$	Experiment active power change	1667.1 W
$Q_{step}$	Experiment reactive power change	795.4 VAR
$h$	Experiment hysteresis band	7000 V/s
$\zeta$	Experiment damping ratio	2

Contrary to the explanation in [7] which attributes this effect to LC filter dynamics and in [20] switching delay of transistors, the simulation in Fig. 4 shows that the delay effect (i.e., switching delay and signal processing delay), the computational error (i.e., specifically the error introduced when the control strategy is implemented in practice rather than an error inherent in the control theory itself), and the potential asymmetric velocity of  $s$  (i.e., caused by asymmetric ac-voltage and ac-current-changing rate in (19)) are reasons of the asymmetry of  $s$  and asymmetric switching dynamics. Reducing  $t_{di}$  to about  $2\mu$ s in Fig. 5 lowers the computational error, consistent with the earlier qualitative prediction. The asymmetry caused by asymmetric switching dynamics creates a great low-frequency-voltage error in Fig. 4 and Fig. 5. If the voltage error at power-line frequency can be suppressed, with the 800 or 900 microseconds convergence speed, this control strategy would have a good voltage tracking performance for synchronization.

The reason why this asymmetry is important is that the smaller the  $\Phi$  is, the smaller the  $|\tilde{x}|$  is. This issue can be seen at these papers [10], [11], where there are low-frequency errors in output voltage whose rippling frequency is the grid frequency. Although the repetitive controller [11] tries to change the sliding surface, but when an instant change occurs, it would lose fast convergence and tracking performance. According to the dominant terms in (17), which is a low-frequency sinusoidal waveform, it is easier to correct the  $s$  by a compensator extracting the asymmetry of  $s$ .

With the symmetric notion above, the desired  $s$  trajectory is given in Fig. 6. The  $s$  dynamics is a function of sample time, control strategy, and physically allowed switching frequency. For example, the dead-band times, sampling process and derivative calculation can cause computation error and switching delay of power semiconductor devices [20], [21]. This

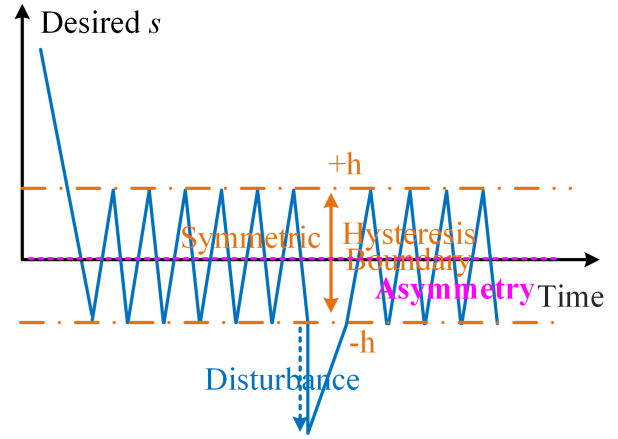


Fig. 6. The ideal  $s$  dynamics, which seems a hysteresis dynamics with a bound.

causes the sliding variable to oscillate around the hysteresis band, creating a persistent offset from the ideal switching surface. Moreover, the asymmetry property of switching behavior in (17) can also damage the symmetry of  $s$  variable.

To address the asymmetrical behavior, the sliding surface is decomposed in (20) into a symmetric dynamic component  $s_{\text{symmetric}}(t)$  which stands for the ideal symmetric sliding surface component shown in Fig. 6, and an error term  $s_{\text{fixed-error}}$  which stands for the asymmetry.

$$s(x, t) = s_{\text{symmetric}} + s_{\text{fixed-error}}$$

$$s_{\text{symmetric}} + s_{\text{fixed-error}} = \left( \frac{d}{dt} + \lambda \right) \tilde{x} \quad (20)$$

$x_{\text{comp}}(t)$  compensator is introduced to eliminate the asymmetry bias, thereby restoring the symmetry of the sliding variable  $s$ , and improving low-frequency tracking accuracy. This proof is shown in (21)

$$\tilde{x} := x - x_d + x_{\text{comp}}$$

$$\text{s.t. } \frac{dx_{\text{comp}}}{dt} + \lambda x_{\text{comp}} = s_{\text{fixed-error}}$$

$$\text{Thus, } \left( \frac{d}{dt} + \lambda \right) (x - x_d) = s_{\text{symmetric}} \quad (21)$$

To extract the low-frequency component of the sliding variable, a second-order band-pass filter is employed. The general form of the filter is given by:

$$H(s) = \frac{2\zeta\omega_0 s}{s^2 + 2\zeta\omega_0 s + \omega_0^2} \quad (22)$$

where  $\omega_0$  is the natural (center) frequency in rad/s, and  $\zeta$  is the damping ratio.

This filter structure extracts the slow-varying envelope of the sliding variable, suppressing the low-frequency switching components. With the saturation input block at the input of this transfer function, this suppression function can only be activated when the sliding variable reaches the around the hysteresis band without losing the fast converging behavior outside the hysteresis boundary. Its effectiveness is shown in Fig. 7 and Fig. 8, which show a better tracking accuracy and the compensated  $s$ , namely  $s_{\text{symmetric}}$  has a lower asymmetry.

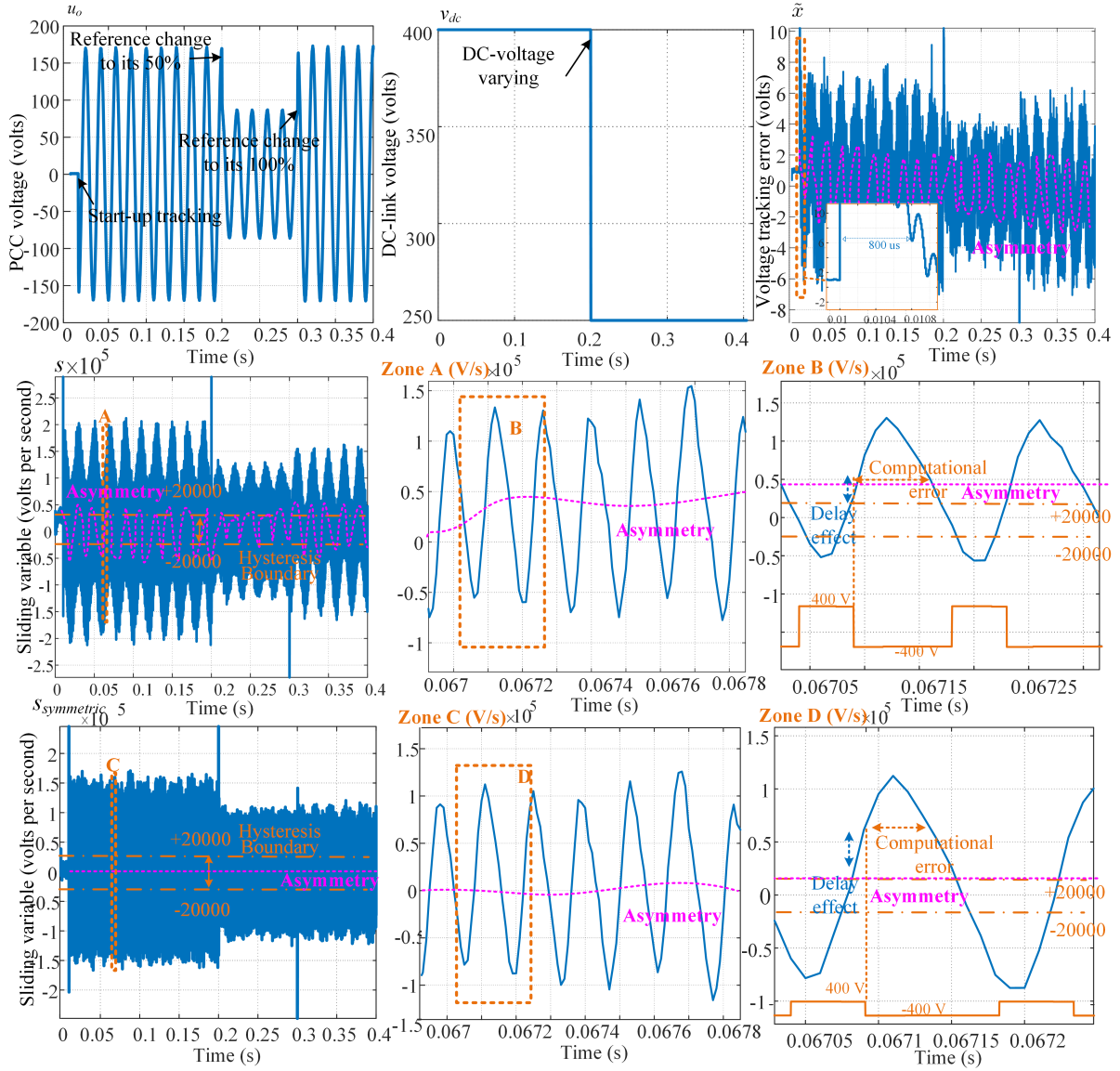


Fig. 7. The simulation result of the proposed symmetric sliding-mode control when  $t_{di} = 10 \mu s$ , with a reference magnitude that steps from 100% to 50% at 0.2s with dc-voltage jump from 400V to 250V for examining the  $v_{dc}$  varying resilience and then back to 100% at 0.3s.

Note that this compensator might cause a little damping-convergence effect if the  $\zeta$  is small. So, the larger  $\zeta$  is better unless the  $s_{fixed-error}$  cannot be extracted efficiently.

### III. EXPERIMENTAL VALIDATION

To verify the proposed symmetric sliding-mode control (SSMC) strategy, a series of experiments are conducted to evaluate the finite-time, almost no low-frequency error voltage tracking performance and its voltage controllable region against ac-side and dc-link large varying. The experimental setup and procedures are designed to simultaneously demonstrate the effectiveness of tracking control and decoupling.

The experiments are conducted on a laboratory-scale grid-forming inverter prototype controlled by the proposed SSMC. Some experimental parameter setups are listed in Table I, several of which remain unchanged from the simulation configuration. The inverter is connected to a programmable AC

source, a controllable load bank, and a programmable DC supply to emulate AC power and dc-link voltage variations, shown in Fig. 9.

Three cases are examined and results are shown in Fig. 10.

- 1) **Case 1 DC-Link Large Varying Test:** A dc-link voltage changing from 150 volts to 180, both don't satisfy the condition (8) and have distortions of the output voltage. After increasing the voltage to 200, 300 and 400 volts, the output voltage is accurately controlled with a tracking error within  $\pm 5$  V. The asymmetry is about  $\pm 1$  V compared with higher asymmetry of the traditional method without symmetry compensation in [10], [11]. Meanwhile, the tracking error data during a 0.02 seconds is extracted in case 1, Fig. 10, which shows a lower low-frequency-voltage oscillation due to the compensation for symmetry compared to 10 V asymmetry by traditional sliding [15]. Compared to [4], no more than 10% dc-link voltage chang-

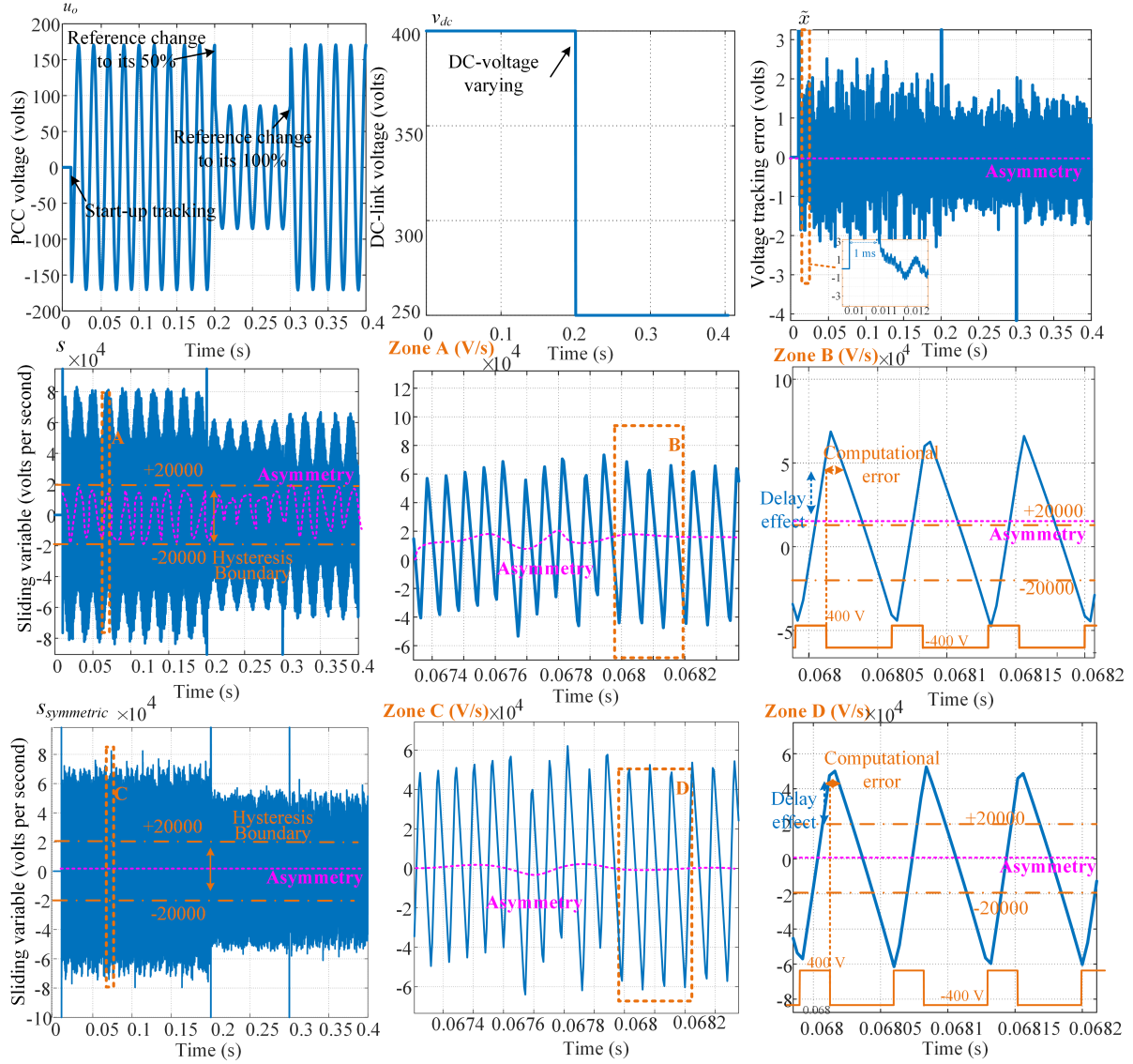


Fig. 8. The simulation result of the proposed symmetric sliding-mode control when  $t_{di} = 2 \mu s$ , with a reference magnitude that steps from 100% to 50% at 0.2s with dc-voltage jump from 400V to 250V for examining the  $v_{dc}$  varying resilience and then back to 100% at 0.3s.

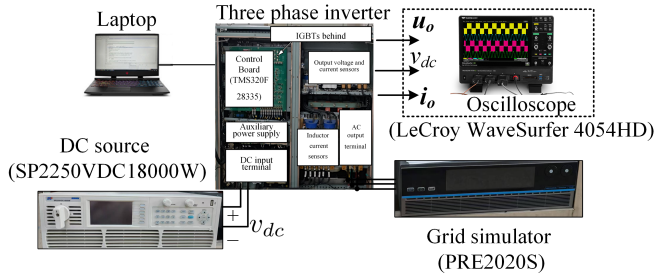


Fig. 9. Experimental setup.

ing can cause intensive interaction between dc voltage control and ac control [4], it shows a decoupling effect of 50% dc-link voltage changing of SSMC and the effectiveness of the controllable region which can predict when the interaction intensifies. For current changing rate resilience

proof, one can refer to [19].

- 2) **Case 2 Step Reference Voltage Test:** A sudden step change (90 degrees phase change and voltage drop to its half and back to the nominal value) is applied to the voltage reference. This PCC voltage regulation task can be seen in many grid voltage drop conditions and be as a scenario to test fast PCC voltage support of GFM control [1]–[3]. The response time could be within 900 microseconds with a smaller overshoot than the high overshoots in methods [10], [11]. This experiment shows that the proposed SSMC has a shorter 1.2ms convergence speed, compared to the [22], where the rise time of PCC voltage is about 10ms.
- 3) **Case 3 AC-Side Varying Test :** A sudden current change (1.8kVA apparent power) is applied on the AC side. The voltage waveform and tracking response are shown. Also, the power dynamics is shown in Fig. 10. Compared to [23] which shows an abrupt 3 A current change of a



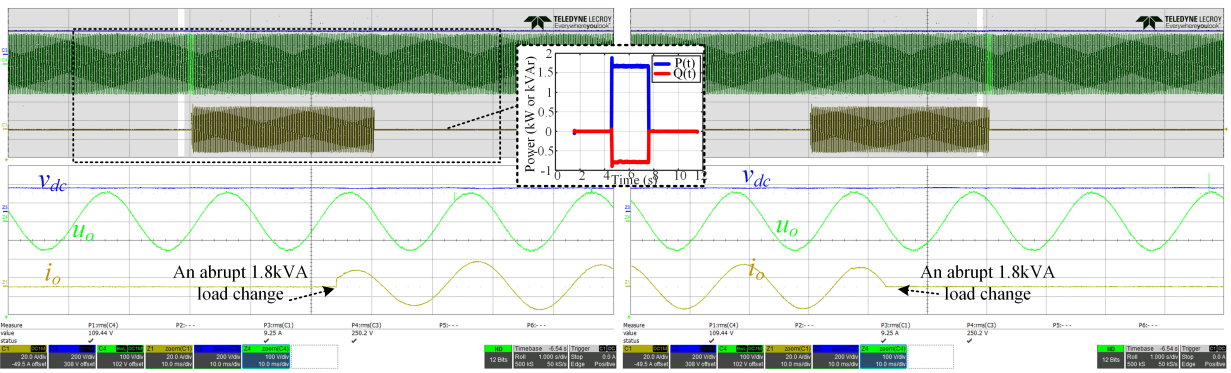
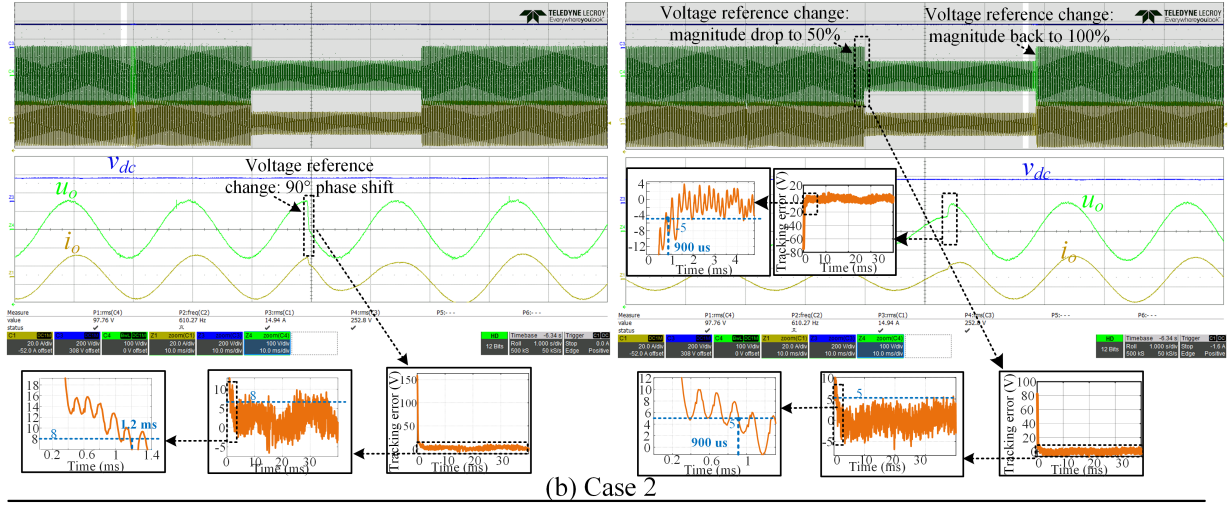
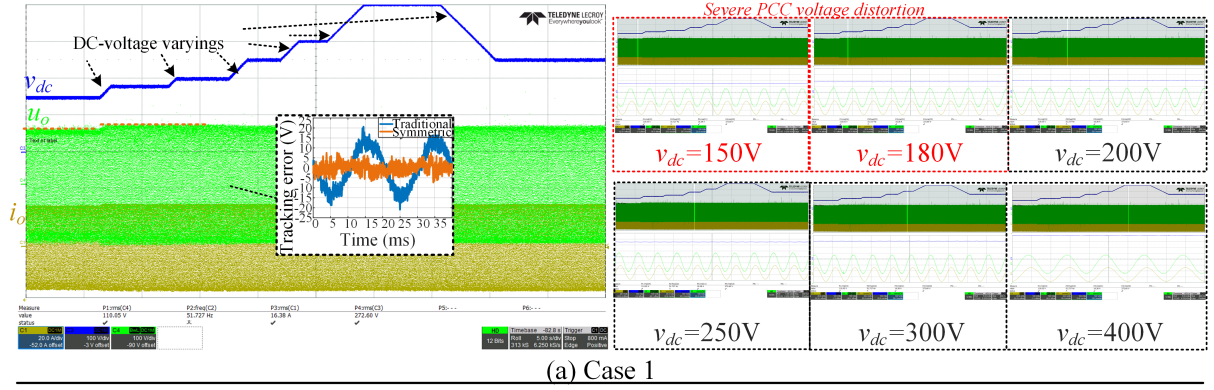


Fig. 10. Comparative experimental validation of the symmetric sliding-mode controller (SSMC). (a) **Case 1-DC-link large varying**: The DC-link voltage is swept from 150V to 400V (150V and 180V are outside the controllable region and then raised to 200V, 250V, 300V, and 400V). (b) **Case 2-step reference voltage**: A sudden  $90^\circ$  phase shift together with a 50 % magnitude drop and 100 % recovery. (c) **Case 3-AC-side varying**: An abrupt 1.8 kVA load change on the AC side.

traditional GFM, the proposed SSMC achieves accurate tracking within  $\pm 5$  V instantaneous error. SSMC has a better AC current resilience performance by fact that it has no transient time of 18 A-AC current varying compared to 10 ms transient time of 10 A-AC current varying in [11]. More about ac-side resilience comparisons by simulation can be referred to [12].

The above proves a decoupled cross-impact between ac-side and dc-link varyings due to control decoupling and superior performance of SSMC over conventional control

under large operating condition varying. With the notion and explicit expression of voltage controllability boundary condition, the loss of voltage regulation can be predicted.

#### IV. CONCLUSION

This paper proposed a symmetric sliding-mode control (SSMC) strategy for grid-forming inverters that explicitly decouples ac-side power dynamics and dc-link voltage varyings from the voltage regulation task. A physical and quantitative explanation aids in designing control parameters. After the



investigation of the root causes of the asymmetry of sliding variable, by decomposing the sliding surface into a symmetric dynamic component and a fixed error term, the proposed method effectively compensates for persistent low-frequency tracking errors caused by the delay effect, the computational error, and the potential asymmetric velocity of  $s$  variable. Experimental results validate the  $900\ \mu\text{s}$  converging performance and dc-ac-varying resilience of the proposed method, particularly under changes in voltage reference, load, and dc-link voltage. With the controller explicit voltage controllability boundary, the voltage regulation ability can be predicted as a well-defined convergence rate and steady-state error. Nevertheless, this work moves beyond the familiar pursuit of "faster-and-cleaner" voltage tracking and instead introduces a closed-form controllable region that links dc-bus excursions and ac-current transients directly to PCC voltage stability. For theory, this boundary exposes the physical mechanism that triggers loss of grid-forming behavior and offers a potential unified yardstick for comparing future GFM strategies. For engineering practice, it supplies an immediate design margin for how far real-world dc and ac variations can be pushed before those performance promises break down.

## REFERENCES

- [1] D. Ríos-Castro, D. Pérez-Estévez, and J. Doval-Gandoy, "Ac-voltage controller for grid-forming converters," *IEEE Transactions on Power Electronics*, vol. 38, no. 4, pp. 4529–4543, 2023.
- [2] Z. Li, C. Zang, P. Zeng, H. Yu, S. Li, and J. Bian, "Control of a grid-forming inverter based on sliding-mode and mixed  $H_2/H_\infty$  control," *IEEE Transactions on Industrial Electronics*, vol. 64, no. 5, pp. 3862–3872, 2017.
- [3] D. B. Rathnayake, S. P. Me, R. Razzaghi, and B. Bahrani, " $H_\infty$ -based control design for grid-forming inverters with enhanced damping and virtual inertia," *IEEE Journal of Emerging and Selected Topics in Power Electronics*, vol. 11, no. 2, pp. 2311–2325, 2023.
- [4] Z. Zeng, P. M. Gajare, D. Divan, and M. Saeedifard, "Impact of dc voltage reference on subsynchronous dynamics in grid-forming inverters," *IEEE Transactions on Power Electronics*, vol. 40, no. 7, pp. 8934–8938, 2025.
- [5] J. Liu, Y. Xia, W. Wei, Q. Feng, and P. Yang, "Effect of control damping on small-signal stability of grid-forming vscs considering interaction between inner and outer loops," *IEEE Transactions on Power Electronics*, vol. 39, no. 6, pp. 7685–7695, 2024.
- [6] T. Liu and X. Wang, "Physical insight into hybrid-synchronization-controlled grid-forming inverters under large disturbances," *IEEE Transactions on Power Electronics*, vol. 37, no. 10, pp. 11 475–11 480, 2022.
- [7] L. Zhao, Z. Jin, and X. Wang, "Small-signal synchronization stability of grid-forming converters with regulated dc-link dynamics," *IEEE Transactions on Industrial Electronics*, vol. 70, no. 12, pp. 12 399–12 409, 2023.
- [8] C. Luo, X. Ma, T. Liu, and X. Wang, "Adaptive-output-voltage-regulation-based solution for the dc-link undervoltage of grid-forming inverters," *IEEE Transactions on Power Electronics*, vol. 38, no. 10, pp. 12 559–12 569, 2023.
- [9] A. Tayyebi, A. Anta, and F. Dörfler, "Grid-forming hybrid angle control and almost global stability of the dc-ac power converter," *IEEE Transactions on Automatic Control*, vol. 68, no. 7, pp. 3842–3857, 2023.
- [10] J. Fei, Y. Zhu, and M. Hua, "Disturbance observer based fuzzy sliding mode control of pv grid connected inverter," in *2018 5th International Conference on Electrical and Electronic Engineering (ICEEE)*, DOI 10.1109/ICEEE2.2018.8391293, pp. 18–22, 2018.
- [11] L. Zheng, F. Jiang, J. Song, Y. Gao, and M. Tian, "A discrete-time repetitive sliding mode control for voltage source inverters," *IEEE Journal of Emerging and Selected Topics in Power Electronics*, vol. 6, DOI 10.1109/JESTPE.2017.2781701, no. 3, pp. 1553–1566, 2018.
- [12] Q. Tang and L. Peng, "A slack bus grid-forming inverter based on symmetric sliding mode control against power sharing imbalances among microgenerators," in *IECON 2024 - 50th Annual Conference of the IEEE Industrial Electronics Society*, pp. 1–6, 2024.
- [13] B. Lin, L. Peng, K. Yu, and H. Xu, "Harmonic disturbance suppression based on precise shaping of output impedance at selected frequencies for standalone voltage source inverter," *IEEE Transactions on Industry Applications*, vol. 59, no. 6, pp. 6963–6975, 2023.
- [14] J.-J. E. Slotine and W. Li, "Applied nonlinear control," 1991. [Online]. Available: <https://api.semanticscholar.org/CorpusID:106519536>
- [15] K. Rayane, A. Rabhi, B. K. Oubbati, and M. Benzoubir, "Enhanced grid-forming inverter control through integral sliding mode control in a cascaded framework," in *2024 4th International Conference on Smart Grid and Renewable Energy (SGRE)*, DOI 10.1109/SGRE59715.2024.10429007, pp. 1–6, 2024.
- [16] Z. Li, C. Zang, P. Zeng, H. Yu, S. Li, and J. Bian, "Control of a grid-forming inverter based on sliding-mode and mixed  $H_2/H_\infty$  control," *IEEE Transactions on Industrial Electronics*, vol. 64, DOI 10.1109/TIE.2016.2636798, no. 5, pp. 3862–3872, 2017.
- [17] P. Alinaghi Hosseinabadi, S. Mekhilef, H. R. Pota, and M. Ker-madi, "Chattering-free fixed-time robust sliding mode controller for grid-connected inverters under parameter variations," *IEEE Journal of Emerging and Selected Topics in Power Electronics*, vol. 12, DOI 10.1109/JESTPE.2023.3336186, no. 1, pp. 579–592, 2024.
- [18] S. Saetieo, R. Devaraj, and D. Torrey, "The design and implementation of a three-phase active power filter based on sliding mode control," *IEEE Transactions on Industry Applications*, vol. 31, DOI 10.1109/28.464511, no. 5, pp. 993–1000, 1995.
- [19] Q. Tang and L. Peng, "Theoretical grid-forming extreme of inverters," 2025. [Online]. Available: <https://arxiv.org/abs/2504.20367>
- [20] O. Kukrer, H. Komurcugil, and A. Doganalp, "A three-level hysteresis function approach to the sliding-mode control of single-phase ups inverters," *IEEE Transactions on Industrial Electronics*, vol. 56, no. 9, pp. 3477–3486, 2009.
- [21] S. Sasitharan and M. Mishra, "Constant switching frequency band controller for dynamic voltage restorer," *IET Power Electronics*, vol. 3, pp. 657–667, 2010. [Online]. Available: <https://digital-library.theiet.org/doi/abs/10.1049/iet-pel.2008.0267>
- [22] F. Zhao, X. Wang, Z. Zhou, Y. Sun, L. Harnefors, and T. Zhu, "Robust grid-forming control with active susceptance," *IEEE Transactions on Power Electronics*, vol. 38, DOI 10.1109/TPEL.2022.3223511, no. 3, pp. 2872–2877, 2023.
- [23] A. Oshnoei, H. Sorouri, R. Teodorescu, and F. Blaabjerg, "An intelligent synchronous power control for grid-forming inverters based on brain emotional learning," *IEEE Transactions on Power Electronics*, vol. 38, DOI 10.1109/TPEL.2023.3300699, no. 10, pp. 12 401–12 405, 2023.

PLACE  
PHOTO  
HERE

**Qianxi Tang** (Graduate Student Member, IEEE) received the B.Eng. degree from the School of Electrical Engineering, Beijing Jiaotong University (BJTU), Beijing, China, in July 2022.

He is currently pursuing the Ph.D. degree with the State Key Laboratory of Advanced Electro magnetic and Technology, School of Electrical and Electronic Engineering, Huazhong University of Science and Technology (HUST), Wuhan, China. His research interests are controls in complex systems, networked systems with ap-

plications to smart power grids, the freedom and limitation of power electronics devices in power system.

Dr. Tang is a reviewer for the IEEE Transactions on Industrial Electronics, a member of the IEEE Power Electronics Society, IEEE Industrial Electronics Society and IEEE Young Professionals. He received the Best Presentation Recognition Award at IECON 2024.

PLACE  
PHOTO  
HERE

**Li Peng** (Senior Member, IEEE) received the B.S., M.S., and Ph.D. degrees in power electronics from the Huazhong University of Science and Technology (HUST), Wuhan, China, in 1989, 1992, and 2004, respectively.

In 1992, she joined HUST, where she is currently a Full Professor of Power Electronics with the School of Electrical and Electronic Engineering. Her research interests include power electronic conversion, its control and applications, modular power supply and parallel control technique, renewable energy generation, power quality control, and modular multilevel converters for high-voltage direct-current applications.